

## A Simple Spike Train Decoder Inspired by the Sampling Theorem

David A. August

William B Levy

Department of Neurosurgery, University of Virginia,  
Charlottesville, VA 22908 USA

Reconstructing a time-varying stimulus estimate from a spike train (Bialek's "decoding" of a spike train) has become an important way to study neural information processing. In this paper, we describe a simple method for reconstructing a time-varying current injection signal from the simulated spike train it produces. This technique extracts most of the information from the spike train, provided that the input signal is appropriately matched to the spike generator. To conceptualize this matching, we consider spikes as instantaneous "samples" of the somatic current. The Sampling Theorem is then applicable, and it suggests that the bandwidth of the injected signal not exceed half the spike generator's average firing rate. The average firing rate, in turn, depends on the amplitude range and DC bias of the injected signal. We hypothesize that nature faces similar problems and constraints when transmitting a time-varying waveform from the soma of one neuron to the dendrite of the postsynaptic cell.

### 1 Introduction

---

Recently, Bialek and colleagues have popularized the "decoding" approach for studying neuronal information processing (Bialek *et al.* 1991; Bialek and Rieke 1992; de Ruyter van Steveninck and Bialek 1988). To describe their method generically, let  $s(t)$  be a time-varying scalar representing a stimulus. In response to this stimulus, the neuron emits a sequence of impulses,  $\{t_i\}$ , which mark each time of spike generation. A decoding filter,  $h(t)$ , is then applied to the spike train, to obtain a new signal,  $\hat{s}(t)$ , which is a continuous, time-varying estimate of the stimulus. The closer  $\hat{s}(t)$  is to  $s(t)$ , the better the spike train has preserved the stimulus information.

This decoding approach has sparked a renewed interest in neural coding, in part because it offers an excellent way for the experimenter to extract much of the information from a spike train. Here, we propose another decoding technique. As an alternative to the methods of Bialek and colleagues, this method takes into account the relationship between cell

firing and signal bandpass, the role of short-term synaptic modifiability, and a limitation to simple postsynaptic filtering functions.

In previous experiments,  $s(t)$  was an environmental stimulus, external to the organism. However, in this paper, we asked how information might be transmitted between two monosynaptically connected neurons. Thus,  $s(t)$  represented a time-varying current injected into the presynaptic cell. At the postsynaptic site, this information would be *decoded* (by conductance events), and *interpolated* into a continuous (current or voltage) signal. Our estimated signal,  $\hat{s}(t)$ , would thus correspond to the subsynaptic waveform.

Briefly, the decoding method consisted of three steps. First, a current waveform,  $s(t)$ , was injected into a model spike generator, which produced a sequence of interspike intervals (ISIs). Next, these ISIs were translated into a sequence of estimated amplitudes ("samples") of  $s(t)$  by a decoding function based on a natural presynaptic process. Finally, these samples were linearly interpolated into a continuous reconstruction,  $\hat{s}(t)$ .

The decoding method proposed here was quite successful, provided that  $s(t)$  was appropriately matched to the spike generator. To understand what is meant by appropriate matching, we must consider spikes as samples, as above. The Sampling Theorem (Shannon 1949; Nyquist 1928; Whittaker 1915) then implies that to avoid aliasing and to produce the best reconstructions, the stimulus bandwidth should be less than half the average sampling rate (firing rate) of the spike generator. Given a particular input signal bandwidth, appropriate adjustments of the signal's DC offset and its amplitude range could produce this matching.

In what follows, we first describe the reconstruction method. Next, we show how the quality of reconstructions is affected by departures from the ideal conditions of the Sampling Theorem, as well as by the stimulus bandwidth and amplitude range. Finally, we discuss how this method relates to other studies, and the implications for experiments designed to measure information transmission between neurons.

## 2 Methods

---

**2.1 Biological and Theoretical Considerations.** The reconstruction technique proposed in this paper was based on linear interpolation, low-pass-filtered signals with restricted bandwidths, and nonlinear filtering. Linear interpolation was motivated by the desire to restrict memory to just the last spike. Low bandwidths ( $\leq 100$  Hz) were used because somatic signals—which we assume arise from passive dendritic filtering of synaptic inputs—would be bandlimited to approximately 25–200 Hz by typical membrane time constants (5–40 msec). Nonlinear filtering was used in correspondence to the nonlinearity of paired-pulse facilitation (PPF) observed at some synapses (Zucker 1989; Katz and Miledi 1968). PPF, a decreasing function of ISI, acts as a nonlinear filter by decoding

each spike into a different postsynaptic conductance, depending on the position of the most recent spike.<sup>1</sup>

With respect to the three points above, previous studies have differed from the method proposed here. First, previous work used interpolating filters with characteristic nonlinear (biphasic or triphasic) shapes, extending over several interspike intervals (Bialek *et al.* 1991; Theunissen 1993). To implement such functions each spike would have to trigger stereotyped event patterns (e.g., fast-EPSP followed by slow-IPSP for a biphasic shape). It remains to be seen whether the proper, stable EPSP/IPSP patterns are generally available at appropriate synapses in the brain, although the implications of this possibility have been noted by several authors (Bialek *et al.* 1991; Sakuranaga *et al.* 1987). Second, previous studies have employed input bandwidths of 500–1000 Hz (Reike *et al.* 1992, 1993; Bialek *et al.* 1991), which were several times higher than average firing rates in most brain regions. While these sensory signals would certainly be lowpass-filtered by (nonauditory) sensory receptors, the filtered bandwidths, in relation to average firing rates, have not been measured. Finally, most previous studies (with the exception of an analysis of bullfrog sacculus data by Reike *et al.* 1992) have used linear, rather than nonlinear, filtering.

**2.2 Reconstruction Method.** We used GENESIS (Bower and Beeman 1995) to simulate the injection of random, time-varying current signals into a biophysically modeled soma. The model, a one-compartment cylindrical soma with sodium and delayed-rectifier potassium channels, is described in Tables 1 and 2. These channel parameters were based on the Hodgkin–Huxley squid axon model (Hodgkin and Huxley 1952). The simulation timestep was  $\Delta t = 30.51758 \mu\text{sec}$ , and the duration of each signal was 1 sec (or  $2^{15} = 32,768$  points).

Current injection signals had the form  $s(t) = i_0 + ai(t)$ , where  $i_0$  was the DC bias,  $a$  was the amplitude scaling factor, and  $i(t)$  was a bandlimited gaussian noise signal. The signal  $i(t)$  was created by lowpass-filtering 32,768 samples of uncorrelated zero-mean, unit variance gaussian white noise, and then rescaling this signal to the  $[-1, 1]$  interval. Filtering was done in the discrete frequency domain, by setting Fourier coefficients above the desired bandwidth to zero. Since each signal was generated

<sup>1</sup>Linear interpolation is like convolving each sample with a triangle-shaped filter, centered around each spike, and extending to the two nearest neighboring spikes. However, because of the PPF-like effect, each triangle has a different height. Thus, convolving the spike train with different-sized triangle functions is actually a nonlinear filtering operation. Thus, in the terminology of this study, the word “linear” has been used in two ways. The triangle-shaped decoding filter was a nonlinear filter. That is, its shape, when centered over the current spike,  $t_i$ , actually depended upon spikes located at  $t_{i-1}$  and  $t_{i+1}$ , violating the superposition property of linear systems. However, the resulting reconstruction,  $\hat{s}(t)$ , was actually a piecewise linear function of time. Most other studies have used linear filtering of spike trains to produce nonlinear reconstruction functions (e.g., Bialek *et al.* 1991; Warland *et al.* 1992; Theunissen 1993).

Table 1: Model Parameters.<sup>a</sup>

Parameter	Description	Value
$d$	Cylinder diameter	500 $\mu\text{m}$
$l$	Cylinder length	500 $\mu\text{m}$
$R_m$	Membrane resistivity	40,000 $\Omega\text{-cm}^2$
$C_m$	Membrane capacitance	1 $\mu\text{F/cm}^2$
$E_r$	Resting potential	-60 mV
$E_{\text{Na}}$	Sodium reversal potential	55 mV
$E_K$	Potassium reversal potential	-72 mV
$\bar{g}_{\text{Na}}$	Sodium channel density	120 mS/cm <sup>2</sup>
$\bar{g}_K$	Potassium channel density	36 mS/cm <sup>2</sup>

<sup>a</sup>The reversal potentials and channel densities correspond to the original Hodgkin-Huxley model for a squid motor axon.

Table 2: Channel Parameters for Na and K Channels in the Hodgkin-Huxley Spike Generator.<sup>a</sup>

Parameter	A	B	C	D	F
$\alpha_m$	$0.1(E_r + 25)$	-0.1	-1	$-(E_r + 25)$	-10
$\beta_m$	4	0	0	$-E_r$	18
$\alpha_h$	0.07	0	0	$-E_r$	20
$\beta_h$	1	0	1	$-(E_r + 30)$	-10
$\alpha_n$	$0.01(E_r + 10)$	-0.01	-1	$-(E_r + 10)$	-10
$\beta_n$	0.125	0	0	$-E_r$	80

<sup>a</sup>To be consistent with GENESIS, each equation for  $\alpha$  or  $\beta$  is written with five parameters, indicating the functional form  $(A + BV)/(C + e^{(V+D)/F})$ . Here,  $E_r$  is the resting potential, -60 mV. The sodium and potassium channel conductances are given by  $g_{\text{Na}} = \bar{g}_{\text{Na}}m^3h$  and  $g_K = \bar{g}_Kn^4$ , respectively, where the gating variable  $u = m, h$ , or  $n$ , obeys the equation  $du/dt = \alpha_u(1 - u) - \beta_u u$ .

with a different random number seed,  $s(t)$  (for a given  $i_0$ ,  $a$ , and bandwidth  $W$ ) were realizations of a bandlimited gaussian random process. We chose a gaussian distribution because, by the central limit theorem, the dendritic filtering of many synaptic inputs would be expected to approach a gaussian at the soma.

The decoding function, which translated ISIs into estimates of the stimulus, was constructed empirically in the following manner. First, 10 different gaussian signals were injected into the spike generator. From the 10 resulting spike trains, each ISI ( $ISI_i = t_i - t_{i-1}$ ), as well as each instan-

taneous current injection,  $s(t_i)$ , was recorded. These pairs of  $(ISI_i, s(t_i))$  produced a scatterplot, like the one shown in Figure 2. The inverting function was obtained by fitting this scatter of points, using Mathematica, to a third-degree polynomial  $f(ISI) = c_0 + c_1/ISI + c_2/ISI^2 + c_3/ISI^3$ .

The reconstruction method was tested by injecting novel signals, generated with different random seeds, into the model spike generator. The inverting function transformed each new spike train into a sequence of "samples"  $\hat{s}(t_i) = f(ISI_i)$  corresponding to the instantaneous current at each spike time. To create a continuous signal,  $\hat{s}(t)$ , these samples were linearly interpolated. That is, for  $t_{i-1} \leq t \leq t_i$ ,

$$\hat{s}(t) = \hat{s}(t_{i-1}) + \frac{\hat{s}(t_i) - \hat{s}(t_{i-1})}{ISI_i}(t - t_{i-1}) \quad (2.1)$$

The reconstruction error between the original and estimated signals was then quantified using relative root-mean-square error (rRMSE),

$$rRMSE = \sqrt{\frac{\langle [\hat{s}(t) - s(t)]^2 \rangle}{\langle s^2(t) \rangle}} \quad (2.2)$$

and, in dB, signal-to-error ratio (SER), defined as  $SER = -20 \log_{10}(rRMSE)$ , where  $\langle \rangle$  denotes a time average.

**2.3 Relationship to Sampling Theorem.** The Sampling Theorem states that a signal bandlimited to  $W$  Hz, uniformly sampled at a rate of  $1/T$ , can be exactly reconstructed from the samples, provided that  $(1/T) > 2W$ . The reconstruction is obtained from

$$\hat{s}(t) = \sum_i s(iT) \text{sinc}[W(t - iT)] \quad (2.3)$$

where  $\text{sinc}(x) = \sin(\pi x)/(\pi x)$ . The just described neuronal ("scatterplot") method reconstructs a continuous signal from the samples  $\hat{s}(t_i) = f(t_i - t_{i-1})$  according to the formula

$$\hat{s}(t) = \sum_i \hat{s}(t_i) \Lambda(t - t_i, t_{i-1}, t_{i+1}) \quad (2.4)$$

where  $\Lambda(\cdot)$  is the triangle function,

$$\Lambda(t, a, b) = \begin{cases} 1 + (t/a), & -a \leq t < 0 \\ 1 - (t/b), & 0 \leq t < b \\ 0, & \text{otherwise} \end{cases} \quad (2.5)$$

Clearly, these two reconstruction techniques are conceptually similar. However, the neuronal ("scatterplot") method differed from the Sampling Theorem in three important ways: The scatterplot method used nonuniform, rather than uniform, sampling; linear, rather than nonlinear, interpolation, and estimated, rather than exact, sample amplitudes.

Table 3: Comparing Different Reconstruction Methods.<sup>a</sup>

	Sampling interval	Interpolation method	Sample amplitudes	Difference(s) from Sampling Theorem		
				NUS	LI	EST
SC	Nonuniform	Linear	Estimated	×	×	×
1	Uniform	Linear	Estimated	—	×	×
2	Nonuniform	Linear	Exact	×	×	—
3	Nonuniform	Nonlinear	Estimated	×	—	×
4	Uniform	Linear	Exact	—	×	—
5	Uniform	Nonlinear	Estimated	—	—	×
6	Nonuniform	Nonlinear	Exact	×	—	—
ST	Uniform	Nonlinear	Exact	—	—	—

<sup>a</sup>The scatterplot reconstruction method, (SC), differed from the Sampling Theorem (ST), in three ways: nonuniformly spaced samples (NUS), linear interpolation (LI), and estimated sample amplitudes (EST). To evaluate the contribution of each of these error sources individually and in pairs, six additional reconstruction methods were employed. Methods 4, 5, and 6 differ from the Sampling Theorem in just one way, while methods 1, 2, and 3 differ in two ways.

**2.4 Analysis of Reconstruction Error.** We wished to compare the error of our neuronally inspired reconstruction method to the theoretical lowest possible error predicted by the Sampling Theorem. However, because our procedure departed from the theorem in three respects, a direct comparison was not meaningful. Therefore, we implemented six other reconstruction methods, as shown in Table 3. Each of these methods differed from the Sampling Theorem in either one or two respects. Thus, for example, comparing methods 4, 5, or 6 to the Sampling Theorem (ST) demonstrated the individual effects of linear interpolation, estimated sample amplitudes, and nonuniform sampling, respectively. Comparing methods 1, 2, or 3 to the Sampling Theorem showed the combined effect of pairs of these error sources. Finally, comparing the scatterplot method (SC) to the Sampling Theorem illustrated the combined effect of all three error sources.

The reconstruction methods are named and described as follows: (ST) A direct implementation of the Sampling Theorem, in which the original signal was sampled uniformly (at the spike train's average firing rate) and these sample points were interpolated with sinc-functions. The resulting error was the lowest possible, given the limitations of finite length signals, non-brickwall filters, and finite precision calculations. (1) Linear interpolation of uniformly spaced, estimated samples. In this method, the exact sample amplitudes from the method above were corrupted by additive, zero-mean, gaussian white noise. The variance of this noise, 72.25 nA, was estimated by averaging the variance from 25 different ISI

bins along the scatterplot, each 0.1 msec in width. (2) A method in which exact nonuniformly spaced samples, taken from the original signal, were linearly interpolated. As sample points, we could have chosen the actual spike times produced by a current injection. However, this would have led to oversampling of the waveform peaks (when the spike generator sped up) and undersampling waveform troughs. To avoid this bias, but still retain the same ISI distribution, we simply used the spike times produced by one current injection,  $s_i(t)$ , to sample a different signal,  $s_j(t)$ . (3) A reconstruction technique for nonlinear interpolation of nonuniformly spaced samples based on Yen's method (Yen 1956), which used variable sinc-functions. In this case, estimated, rather than exact, sample amplitudes were used. Again, these corrupted amplitudes were produced by adding  $N(0, 72.25)$  noise to the original amplitudes.<sup>2</sup> (4) A method in which exact, uniformly spaced samples were connected by straight lines, rather than sinc-functions. (5) The Sampling Theorem applied to uniformly spaced sample amplitudes, corrupted by  $N(0, 72.25)$  noise. (6) Yen's method applied to nonuniformly spaced, exact sample amplitudes, taken directly from the original signal at the specified times.

The rRMSE of the scatterplot method (see Table 3) was denoted  $E_{SC}$ ; the rRMSE of the Sampling Theorem implementation was denoted  $E_{ST}$ ; the other rRMSE's were denoted  $E_1, E_2, \dots, E_6$ , corresponding to the six reconstruction methods above. To interpret the total error,  $E_{SC}$ , in the context of the Sampling Theorem, each of the above reconstruction errors was first normalized by  $E_{SC}$ . Then, the closer a given normalized error ratio was to 1, the more of  $E_{SC}$  was explained by that particular departure (or departures) from the Sampling Theorem.

### 3 Results

**3.1 Steady-State Behavior.** Before injecting time-varying current signals, we studied the steady-state behavior of the Hodgkin-Huxley model by constructing a frequency-intensity ( $f/I$ ) curve, shown in Figure 1. Consistent with previous reports (Agin 1964; Stein 1967), the model spike generator abruptly began repetitive firing at about 50 Hz, rose to a maximum of 170 Hz, and declined sharply.

<sup>2</sup>Although in theory Yen's third method produces perfect reconstructions, in practice it is extremely sensitive to amplitude errors. Indeed, these facts may have been known to Cauchy in 1841 (see Black 1953; Jerri 1977; Marks 1991), and were certainly known to Shannon, who wrote, "[t]he 2WT numbers used to specify the function need not be the equally spaced samples. . . . For example, the samples can be unevenly spaced, although, if there is considerable bunching, the samples must be known very accurately to give a good reconstruction of the function" (Shannon 1949).

We have found that the requirement for high accuracy renders Yen's third method useless in practice. However, Yen's fourth method, which applies the constraint of minimum energy, can produce reasonable reconstructions. Accordingly, all references to Yen's method hereafter denote his fourth method.

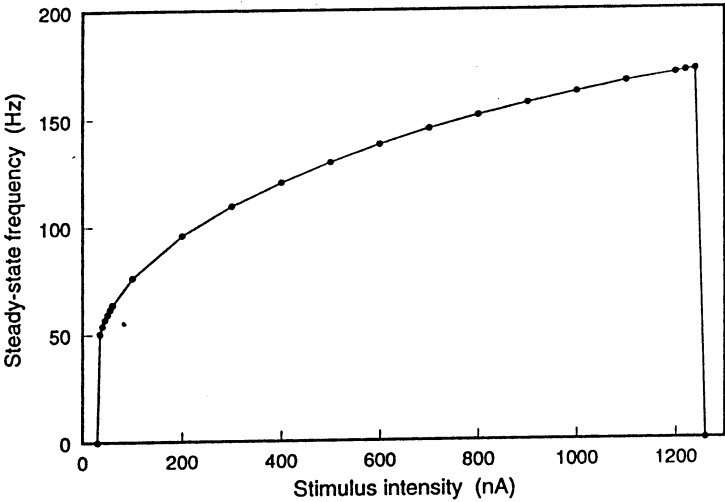


Figure 1: The steady-state frequency/intensity ( $f/I$ ) curve. The model spike generator began firing in response to a 35 nA current injection and eventually reached its maximum response at 1240 nA.

**3.2 The Inverting Curve.** For the first reconstruction experiments, the firing rate was set at  $\approx 100$  Hz by confining the current injection signal to 35–435 nA. That is,  $s(t) = i_0 + ai(t)$ , with  $i_0 = 235$  nA,  $a = 200$  nA, and  $i(t) \in [-1, 1]$ . In order to meet the Nyquist criterion,  $i(t)$  was lowpass-filtered to a 40 Hz bandwidth. Ten such signals were injected into the model spike generator. Figure 2 shows the resulting scatterplot [obtained by plotting  $(ISI_i, s(t_i))$  pairs] and the inverting function,  $f(ISI)$ .

**3.3 Reconstruction Error and the Sampling Theorem.** Next, 10 novel 40 Hz gaussian signals were reconstructed using this inverting curve. Figure 3 shows one representative reconstruction (rRMSE = 0.3648). For all ten signals, the quality of reconstructions was similarly high, with  $rRMSE = 0.3623 \pm 0.0121$ , and  $SER = 8.8636 \pm 0.2950$  dB.

To estimate how much of this error was due to the various departures from the Sampling Theorem, the signals were also reconstructed using the techniques shown in Table 3. The average rRMSEs for these different reconstruction methods are given in Table 4.

Comparing methods 4, 5, and 6 to the method ST shows the effect of individual departures from the Sampling Theorem. Since  $E_4/E_{SC} = 0.89$  was the highest error ratio, linear interpolation was the largest single

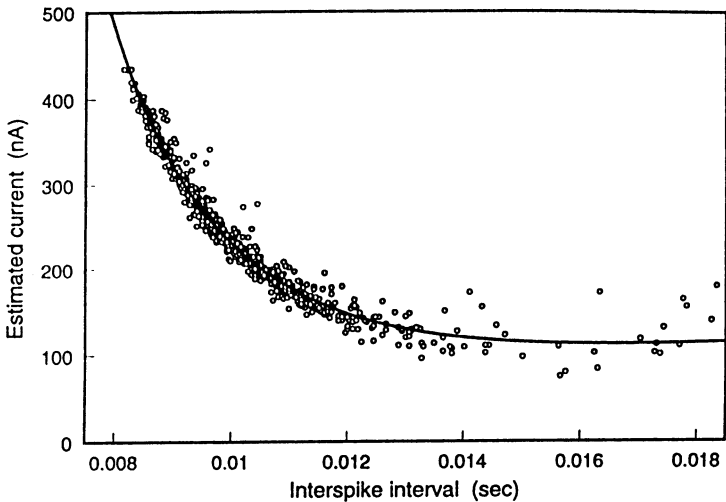


Figure 2: Scatterplot and inverting curve. Pairs of points  $(ISI_i, s(t_i))$  were plotted (open circles) to form a scatterplot. This scatter of 936 points contains data from 10 1-sec long 40-Hz bandlimited gaussian noise signals. To obtain an inverting curve (solid line), this scatter of points was fit with the function  $f(ISI) = 183.565 - 0.433928/ISI - 0.0447669/ISI^2 + 0.000538129/ISI^3$ .

source of error. Less of a penalty was paid for nonexact sample amplitudes ( $E_5/E_{SC} = 0.65$ ) and nonuniform sampling ( $E_6/E_{SC} = 0.64$ ). As expected, errors for reconstruction methods that combined linear interpolation with still another departure from the Sampling Theorem (e.g.,  $E_1$  and  $E_2$ ) accounted for almost all of the total error of  $E_{SC}$ .

**3.4 Tuning the Stimulus to the Spike Generator.** We investigated the role of matching the injected current with the spike generator in two ways. First, we held the stimulus bandwidth constant (40 Hz), and varied its amplitude range. We hypothesized that increasing the firing rate (sampling rate) would improve reconstructions. Since the average firing rate was controlled by the DC bias and amplitude of the stimulus, we compared reconstructions from signals restricted to different sections of the  $f/I$  curve. Signals were restricted to either the full (35–435 nA), low (35–335 nA), middle (135–335 nA), or high (135–435 nA) range of the  $f/I$  curve, and a different scatterplot was constructed for each range. The average firing rate for each of these ranges was high ( $106.0 \pm 0.5$  Hz) > middle ( $100.0 \pm 0.3$  Hz) > full ( $95.2 \pm 0.8$  Hz) > low ( $88.1 \pm 0.8$  Hz). Figure 4

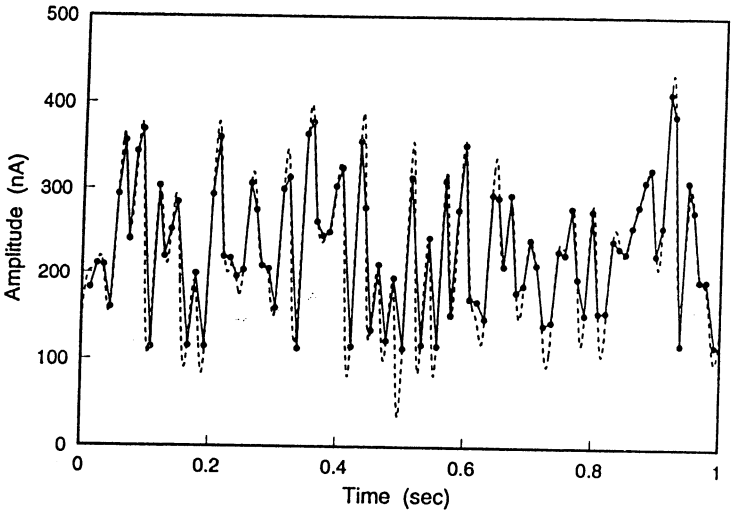


Figure 3: Reconstruction of a time-varying current injection. The original signal (dotted line) was 40-Hz lowpass-filtered gaussian noise with an amplitude range of 35–435 nA. The reconstructed signal (solid line), obtained from the inverting function in Figure 2, had an  $rRMSE$  of 0.3648 and an SER of 8.7587 dB. (See Methods for a description of how to calculate  $rRMSE$  and SER.) This reconstruction was based on 92 pairs of  $(ISI, \hat{s}(t_i))$  points (filled circles).

shows that the reconstruction errors were ranked in the opposite order to the firing rates:  $rRMSE_{high} < rRMSE_{middle} < rRMSE_{full} < rRMSE_{low}$ . Thus, larger DC bias, which produced higher firing rates, also produced better reconstructions, in agreement with the Sampling Theorem idea.

The second type of stimulus/spike-generator matching was tested by holding the stimulus amplitude constant (135–435 nA), and varying its bandwidth. Since current injections in this range produced average firing rates of 106 Hz, we hypothesized that stimuli bandlimited to less than 53 Hz would be reconstructed better than those with larger bandwidths. To test this, we compared reconstructions from 20, 40, 60, and 80 Hz bandlimited gaussian noise signals. Again, a different scatterplot was constructed for each bandwidth. As shown in Figure 5, reconstruction error increased with the stimulus bandwidth. Aliasing, most pronounced in the Sampling Theorem method, was seen as a sharp increase in the error when the signal's bandwidth was changed from 40 to 60 Hz. Interestingly, the reconstruction methods using linear interpolation degraded more gracefully than the methods using nonlinear interpolation.

Table 4: Reconstruction Errors.<sup>a</sup>

	Difference(s) from Sampling Theorem			rRMSE ( $\pm$ SE)	$E_i/E_{sc}$
	NUS	LI	EST		
SC	×	×	×	$0.239 \pm 0.007$	1.00
1	—	×	×	$0.252 \pm 0.005$	1.05
2	×	×	—	$0.218 \pm 0.004$	0.91
3	×	—	×	$0.164 \pm 0.005$	0.69
4	—	×	—	$0.213 \pm 0.004$	0.89
5	—	—	×	$0.155 \pm 0.006$	0.65
6	×	—	—	$0.153 \pm 0.012$	0.64
ST	—	—	—	$0.009 \pm 0.001$	0.04

<sup>a</sup>For each of the reconstruction methods described in Table 3, the relative RMS error (rRMSE) is given here, along with the SE ( $n = 10$ ). Also shown are errors normalized by the scatterplot method's error,  $E_{sc}$ . Note that linear interpolation (method 4) alone accounts for nearly 90% of the total error. The input signals were scaled to the 135–435 nA range.

#### 4 Discussion

This paper has presented a simple technique for reconstructing a continuous, time-varying signal from a simulated spike train. Although this type of study has often been called “decoding,” we emphasize our agreement with others (Perkel and Bullock 1968; Bialek and Rieke 1992) that neurons need not decode their incoming spike trains. Still, even without the presence of a literal decoder, information is present implicitly in spike trains.

The question motivating the present research is how much information about a bandlimited waveform is preserved given a neuronal spike generator and a hypothesized synaptic decoding process that has memory no further back in time than the previous impulse. The reconstruction method described here is inspired by one biological process (PPF) and by—what is to us—the intuitively appealing restriction of limited temporal inference (no memory for spikes beyond the previous one). Linear interpolation, while no more or less biologically plausible than many other interpolation schemes, is one of the simplest interpolating functions that is consistent with the assumed temporal restriction. Thus, in addition to being a useful tool by which experimenters can decode spike trains, linear interpolation also represents a low complexity information-preserving computation that a synapse might be able to accomplish.

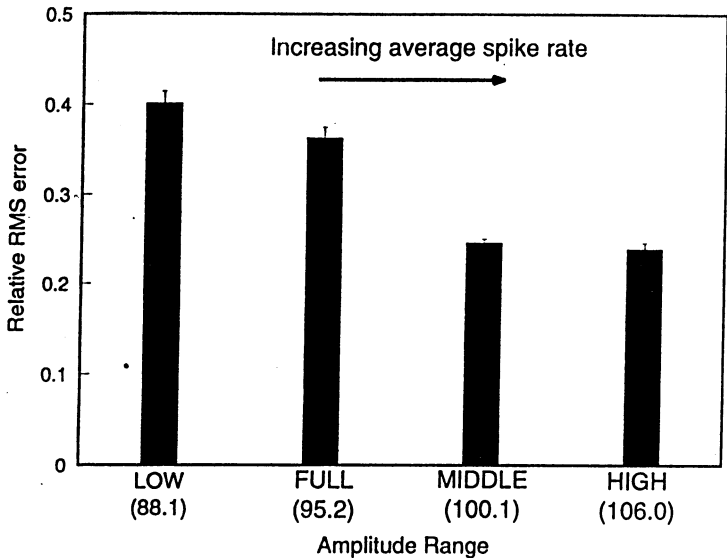


Figure 4: Increasing the firing frequency decreased the reconstruction error. Each bar represents the average rRMSE ( $\pm$  SE) for scatterplot reconstructions of 10 input signals that had the same (40 Hz) bandwidth but were rescaled to different amplitude ranges along the  $f/I$  curve. As the average firing rate increased (from  $\approx 88$  Hz on the left to  $\approx 106$  Hz on the right), the rRMSE decreased. Generally, the firing frequency could be predicted by the mean value (DC level) of the stimulus. However, the average firing rate of “middle” range signals was larger than that of the “full” ( $100.1 \pm 0.3$  Hz vs.  $95.2 \pm 0.8$  Hz), and the rRMSE was smaller, even though they had the same DC bias. Numbers in parentheses below the amplitude ranges correspond to the average firing rate in Hz.

**4.1 Other Spike Generators.** It has been suggested, because the Hodgkin-Huxley spike generator has such a narrow dynamic range (Fig. 1) and a regular firing rate, that the reconstruction method described here may not be generally applicable. However, the same reconstruction technique (August and Levy 1994) has also been applied to spike trains from a retinal ganglion cell (RGC) model (Fohlmeister *et al.* 1990). The wider dynamic range of the RGC model was reflected in a larger coefficient of variance (CV) of the ISI histogram compared to the Hodgkin-Huxley model. For example, the CV of the RGC model, when stimulated with 50 Hz bandwidth gaussian noise, was 0.26. This was over twice the CV of the Hodgkin-Huxley spike generator when stimulated with 40 Hz

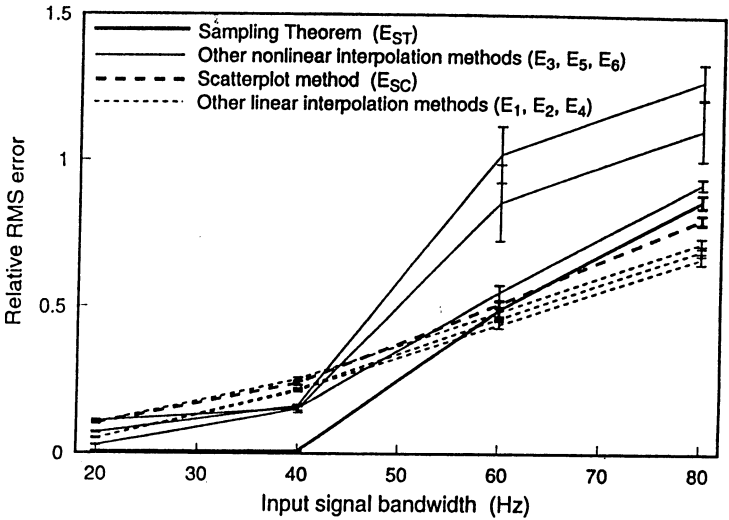


Figure 5: Increasing stimulus bandwidth increased reconstruction error. Signals were scaled to the same (135–435 nA) amplitude range, but were filtered with lowpass cutoffs of 20, 40, 60, or 80 Hz. That is, while average firing frequency remained constant ( $\approx 106$  Hz), the stimulus bandwidth increased. The markedly increased errors for 60 and 80 Hz bandwidths indicate aliasing. Aliasing was most apparent in the reconstruction methods using nonlinear interpolation (solid lines). For the methods using linear interpolation (dashed lines), the increased slope of the rRMSE curve was less apparent.

( $CV = 0.10$ ) or 60 Hz ( $CV = 0.12$ ) noise. Thus, increasing the spike generator's dynamic range and the irregularity of spiking does not invalidate our approach.

**4.2 The Sampling Theorem.** This paper has related information transmission to communication theory by relating the average firing frequency of a neuron to the Sampling Theorem. However, while conceptually similar to a classical Sampling Theorem reconstruction, the method here differed by its use of nonuniformly spaced samples, nonexact sample amplitudes, and linear interpolation. A comparison of several different reconstruction methods (Table 3) revealed how much these three error sources contribute to the total overall error. For the particular signals studied, linear interpolation was the most significant single factor in increasing error (Table 4). However, the exact ranking of these errors may

change depending on the bandwidth and amplitude range of the input signals (data not shown).

Aliasing, as defined for sinc-function reconstructions (Couch 1987), is a type of reconstruction error caused by high-frequency signal components being "folded" back into lower frequencies, due to an inadequate sampling rate. The Nyquist rate is the sampling rate below which this folding occurs. To investigate the relevance of the Nyquist rate to neuronal communication, we examined the relationship between spike rate and stimulus bandwidth. In varying the firing frequency for a constant stimulus bandwidth (Fig. 4), reconstruction error decreased as firing frequency increased. In varying the input signal bandwidth while maintaining a constant firing frequency (Fig. 5), reconstruction error increased as this bandwidth increased. Thus, relative to communications theory, spike frequency seemed to be the appropriate analog of sampling frequency. Also, the importance of matching this sampling—or spike—frequency to the input signal bandwidth was clearly apparent.

In these aliasing studies, the reconstructions using linear interpolation degraded more gracefully than nonlinear interpolation as input bandwidth increased (Fig. 5). This observation may be biologically pertinent. Since neuronal signals are not strictly bandlimited at these low frequencies, aliasing will likely be present *in vivo*. Thus, it is notable that nature can combat aliasing by simplifying the interpolatory scheme from nonlinear to linear.

The relationship between cell firing and the Nyquist rate has implications for the experimental design of future studies that deliver a time-varying current injection to a neuron, record a spike train, and then "decode" this spike train into an estimate of the stimulus. While much work has gone into determining the appropriate decoding filter, the question of how the stimulus itself should be chosen remains open. Several researchers have already emphasized the complexity of naturalistic stimuli (Field 1987; Ruderman and Bialek 1994). Here, we propose a specific guideline for neurophysiologists. Gaussian current injection signals should be scaled so that the DC bias and amplitude range produce firing at rates comparable to those observed *in vivo*. Next, the stimulus bandwidth should be limited to half this average firing rate or less, if a maximal capacity measurement is the goal.

The relationship of the reconstruction method proposed here, the Sampling Theorem, and other decoding studies can be understood as follows. Bialek and colleagues have shown the theoretical optimality of linear decoding filters when the firing rate,  $\bar{R}$ , becomes very small compared to the stimulus bandwidth,  $W$  (Bialek *et al.* 1993), and this has been confirmed experimentally by decoding sensory system spike trains with linear filters (Bialek *et al.* 1991; Warland *et al.* 1992; Theunissen 1993). Thus, linear decoding filters can be used quite successfully in the  $\bar{R} < 2W$  range of neural dynamics. However, the Sampling Theorem suggests that the  $\bar{R} > 2W$  range of dynamics may also be of interest. In this case, linear decoding

may no longer be optimal, and the experimenter faces the more difficult task of constructing nonlinear filters. The present study shows, empirically, that a very simple (triangular-shaped) nonlinear filter—equivalent to linear interpolation—can still produce high-quality reconstructions. This method should prove useful to experimenters interested in decoding more slowly varying stimuli from spike trains with higher firing rates.

**4.3 Limitations of the Model.** The model of information transmission by ISIs applies to neural systems with a PPF decay similar to the average firing rate, a relatively small conduction jitter, and a relatively large quantal content. We hypothesize that if these conditions are not met, then the spike train is transmitting a frequency code.

First, our reconstruction method requires that the average ISIs for the postsynaptic cell lie along a range of moderate slope on the PPF-like decoding curve (Fig. 2). If ISIs fall predominantly along the nearly flat region, then the EPSPs would all be the same size, as is the case for linear filtering methods (Bialek *et al.* 1991). At the squid giant synapse, the first component of PPF decays over 5–10 msec (Charlton and Bittner 1978), which is suitably matched to the  $\approx 100$  Hz firing rate that has been used here. Similarly, PPF at spinal interneuron–motoneuron and at corticorubral synapses decays over 50 msec (Murakami *et al.* 1977; Kuno and Weakly 1972), which would be appropriate for cells firing at 10–20 Hz.

Second, poor reconstructions could result from ISIs being distorted by a large axonal conduction jitter. Many neural systems have relatively little jitter. For example, in the frog sciatic nerve, jitter is  $\approx 4$   $\mu$ sec, (Rapoport and Horvath 1960),  $< 50$   $\mu$ sec in human motor axons (Salmi 1983; Stralberg *et al.* 1971), 100–200  $\mu$ sec in various reflex arcs (Trontelj 1973; Trontelj and Trontelj 1978),  $< 50$   $\mu$ sec in the barn owl auditory system (Rose *et al.* 1967),  $< 40$   $\mu$ sec in the bat echolocation system (Simmons 1979), and  $< 1$   $\mu$ sec in the weakly electric fish (Bullock 1970). In fact, jitter as a noise source was already implicit in the reconstruction method here. Since the decoding function was fit to a scatterplot, the method must have been robust to *at least* the amount of scatter about this curve. For the 40 Hz signal shown in Figure 2, the widest scatter was approximately 200  $\mu$ sec, which provides a lower bound on the maximum tolerable jitter.

Third, the reconstruction technique will not work at synapses with low and variable quantal content [e.g., hippocampal region CA1 (Allen and Stevens 1994; Bekkers and Stevens 1990; Foster and McNaughton 1991; Hessler *et al.* 1993)], but is applicable where quantal content is high [e.g., squid giant synapse (Miledi 1967), frog neuromuscular junction (Martin 1955), and the climbing fiber synapses on cerebellar Purkinje cells (Llinas *et al.* 1969)]. Because we invoke a PPF-like effect for decoding, and because PPF is thought to be caused by changes in release probability,  $p$ , a fairly large number of release sites,  $n$ , would be required to detect the PPF-induced variability in  $np$ . Further, by emphasizing the importance of individual ISIs for carrying information, we assume reliable synaptic

transmission (e.g.,  $np \gg 1$ , and a high safety factor for spike invasion). Therefore, an explicit conclusion is that systems with low safety factors or low release probability and few release sites will not use ISI codes.

Finally, we note that this study has approached neuronal information transmission differently than nature. We adjusted the stimulus bandwidth and amplitudes to match the spike generator. In nature, however, neurons would presumably co-evolve so that spike generators, interpolators, and dendritic filters matched. That is, we expect that evolution has discovered some simple filtering and interpolation schemes that avoid substantial information loss.

## Acknowledgments

---

This research was supported in part by NIH GM07267 and MH10702 to D.A.A., and NIH MH00622 and MH48161 to W.B.L., and EPRI RP8030-08 to P. Papantoni-Kazakos, and by the Department of Neurosurgery, University of Virginia, Dr. John A. Jane, Chairman. The authors would like to thank Steve Wilson and Chris Fall for their constructive comments.

## References

---

- Agin, D. 1964. Hodgkin-Huxley equations: Logarithmic relation between membrane current and frequency of repetitive activity. *Nature (London)* 201, 625–626.
- Allen, C., and Stevens, C. F. 1994. An evaluation of causes for unreliability of synaptic transmission. *Proc. Natl. Acad. Sci. U.S.A.* 91, 10380–10383.
- August, D. A., and Levy, W. B. 1994. Information maintenance by retinal ganglion cell spikes. In *The Neurobiology of Computation*, J. M. Bower, ed., pp. 41–46. Kluwer, Norwell, MA.
- Bekkers, J. M., and Stevens, C. F. 1990. Presynaptic mechanism for long-term potentiation in the hippocampus. *Nature (London)* 346, 724–729.
- Bialek, W., and Rieke, F. 1992. Reliability and information transmission in spiking neurons. *TINS* 15(11), 428–434.
- Bialek, W., Rieke, F., and de Ruyter van Steveninck, R. 1991. Reading a neural code. *Science* 252, 1854–1857.
- Bialek, W., DeWeese, M., Rieke, F., and Warland, D. 1993. Bits and brains: Information flow in the nervous system. *Physica A* 200, 581–593.
- Black, H. S. 1953. *Modulation Theory*. D. Van Nostrand, New York.
- Bower, J. M., and Beeman, D. 1995. *The Book of Genesis*. Springer-Verlag Telos, New York.
- Bullock, T. H. 1970. The reliability of neurons. *J. Gen. Phys.* 55, 565–584.
- Charlton, M. P., and Bittner, G. D. 1978. Facilitation of transmitter release at squid synapses. *J. Gen. Physiol.* 72, 471–486.
- Couch, L. W. 1987. *Digital and Analog Communication Systems*. Macmillan, New York.

- de Ruyter van Steveninck, R., and Bialek, W. 1988. Real-time performance of a movement-sensitive neuron in the blowfly visual system: Coding and information transfer in short spike sequences. *Proc. R. Soc. London B* **234**, 379–414.
- Field, D. J. 1987. Relations between the statistics of natural images and the response properties of cortical cells. *J. Opt. Soc. Am.* **4**(12), 2379–2394.
- Fohlmeister, J. F., Coleman, P. A., and Miller, R. F. 1990. Modeling the repetitive firing of retinal ganglion cells. *Brain Res.* **510**, 343–345.
- Foster, T. C., and McNaughton, B. L. 1991. Long-term enhancement of CA1 synaptic transmission is due to increased quantal size, not quantal content. *Hippocampus* **1**(1), 79–91.
- Hessler, N. A., Shirke, A. M., and Malinow, R. 1993. The probability of transmitter release at a mammalian central synapse. *Nature (London)* **366**, 569–572.
- Hodgkin, A. L., and Huxley, A. F. 1952. A quantitative description of membrane current and its application to conduction and excitation in nerve. *J. Physiol.* **117**, 500–544.
- Jerri, A. J. 1977. The Shannon sampling theorem—its various extensions and applications: A tutorial review. *Proc. IEEE* **65**(11), 1565–1596.
- Katz, B., and Miledi, R. 1968. The role of calcium in neuromuscular facilitation. *J. Phys.* **195**, 481–492.
- Kuno, M., and Weakly, J. N. 1972. Facilitation of monosynaptic excitatory synaptic potentials in spinal motoneurons evoked by internuncial impulses. *J. Physiol.* **224**, 271–286.
- Llinas, R., Bloedel, J. R., and Hillman, D. E. 1969. Functional characterization of neuronal circuitry of frog cerebellar cortex. *J. Neurophys.* **32**(6), 847–870.
- Marks, R. J. 1991. *Introduction to Shannon Sampling and Interpolation Theory*. Springer-Verlag, New York.
- Martin, A. A. 1955. A further study of the statistical composition of the end-plate potential. *J. Physiol.* **130**, 114–122.
- Miledi, R. 1967. Spontaneous synaptic potentials and quantal release of transmitter in the stellate ganglion of the squid. *J. Physiol.* **192**(2), 379–406.
- Murakami, F., Tsukahara, N., and Fujito, Y. 1977. Properties of synaptic transmission of the newly formed cortico-rubral synapses after lesion of the nucleus interpositus of the cerebellum. *Exp. Brain Res.* **30**, 245–258.
- Nyquist, H. 1928. Certain topics in telegraph transmission theory. *AIEE Trans.* **47**, 617–644.
- Perkel, D. H., and Bullock, T. H. 1968. Neural coding. *Neurosci. Res. Prog. Bull.* **6**(3), 227–348.
- Rapoport, A., and Horvath, W. J. 1960. The theoretical channel capacity of a single neuron as determined by various coding schemes. *Information Control* **3**, 335–350.
- Reike, F., Yamada, W., Moortgat, K., Lewis, E. R., and Bialek, W. 1992. Real time coding of complex sounds in the auditory nerve. *Adv. Biosci.* **83**, 315–322.
- Reike, F., Warland, D., and Bialek, W. 1993. Coding efficiency and information rates in sensory neurons. *Europhys. Lett.* **22**(2), 151–156.
- Rose, J. E., Brugge, J. F., Anderson, D. J., and Hind, J. E. 1967. Phase-locked re-

- sponse to low-frequency tones in single auditory nerve fibers of the squirrel monkey. *J. Neurophys.* 30, 769-793.
- Ruderman, D. L., and Bialek, W. 1994. Statistics of natural images: Scaling in the woods. In *Advances in Neural Information Processing Systems*, J. D. Cowan, G. Tesauro, and J. Alspecter, eds., Vol. 6, pp. 551-558. Morgan Kaufmann, San Mateo, CA.
- Sakuranaga, M., Ando, Y.-I., and Naka, K.-I. 1987. Dynamics of the ganglion cell response in the catfish and frog retinas. *J. Gen. Phys.* 90, 229-259.
- Salmi, T. 1983. A duration matching method for the measurement of jitter in single fibre EMG. *Electroencephalogr. Clin. Neurophysiol.* 56, 515-520.
- Shannon, C. E. 1949. Communications in the presence of noise. *Proc. IRE* 37, 10-21.
- Simmons, J. A. 1979. Perception of echo phase information in bat sonar. *Science* 204, 1336-1338.
- Stalberg, E., Ekstedt, J., and Broman, A. 1971. The electromyographic jitter in normal human muscles. *Electroencephalogr. Clin. Neurophysiol.* 31, 429-438.
- Stein, R. B. 1967. The frequency of nerve action potentials generated by applied currents. *Proc. Royal Soc. London B* 167, 64-86.
- Theunissen, F. E. 1993. *An investigation of sensory coding principles using advanced statistical techniques*. Ph.D. thesis, University of California, Berkeley, Berkeley, CA.
- Trontelj, J. V. 1973. A study of the H-reflex by single fibre EMG. *J. Neurol. Neurosurg. Psych.* 36, 951-959.
- Trontelj, M. A., and Trontelj, J. V. 1978. Reflex arc of the first component of the human blink reflex: a single motoneurone study. *J. Neurol. Neurosurg. Psych.* 41, 538-547.
- Warland, D., Landolfa, M., Miller, J. P., and Bialek, W. 1992. Reading between the spikes in the cercal filiform hair receptors of the cricket. In *Analysis and Modeling of Neural Systems*, F. H. Eeckman, ed., pp. 327-333. Kluwer, Norwell, MA.
- Whittaker, J. M. 1915. On the functions which are represented by the expansion of interpolating theory. *Proc. Math. Soc. Edinburgh* 35, 181-194.
- Yen, J. L. 1956. On nonuniform sampling of bandwidth-limited signals. *IRE Trans. Circ. Theory* CT-3, 251-257.
- Zucker, R. S. 1989. Short-term synaptic plasticity. *Annu. Rev. Neurosci.* 12, 13-31.